

The Influence of Murine Genetic Background in Adeno-Associated Virus Transduction of the Mouse Brain

Ting He,¹ Michelle S. Itano,^{2,3} Lauriel F. Earley,¹ Nikita E. Hall,¹ Natallia Riddick,³ R. Jude Samulski,^{1,4} and Chengwen Li^{1,3,5,*}

¹Gene Therapy Center, University of North Carolina at Chapel Hill, Chapel Hill, North Carolina.

²UNC Neuroscience Center and the Department of Cell Biology and Physiology, University of North Carolina School of Medicine, Chapel Hill, North Carolina.

³Carolina Institute for Developmental Disabilities, University of North Carolina at Chapel Hill, Chapel Hill, North Carolina.

⁴Department of Pharmacology, University of North Carolina at Chapel Hill, Chapel Hill, North Carolina.

⁵Department of Pediatrics, University of North Carolina at Chapel Hill, Chapel Hill, North Carolina.

Adeno-associated virus (AAV) vectors have become an important tool for delivering therapeutic genes for a wide range of neurological diseases. AAV serotypes possess differential cellular tropism in the central nervous system. Although several AAV serotypes or mutants have been reported to transduce the brain efficiently, conflicting data occur across studies with the use of various rodent strains from different genetic backgrounds. Herein, we performed a systematic comparison of the brain transduction properties among five AAV serotypes (AAV2, 5, 7, 8, and 9) in two common rodent strains (C57BL/6J and FVB/N), following local intrastriatal injection of AAV vectors encoding enhanced green fluorescent protein (EGFP) driven by the CBh promoter. Important differences were found regarding overall cellular tropism and transduction efficiency, including contralateral transduction among the AAV serotypes and between the mouse strains. We have further found loss of NeuN-immunoreactivity and microglial activation from AAV transduction in the different mouse strains. The important strain-specific differences from our study suggest that the genetic background of the mouse may affect AAV serotype transduction properties in the brain. These data can provide valuable information about how to choose an effective AAV vector for clinical application and interpret the data obtained from preclinical studies and clinical trials.

Keywords: AAV, serotypes, brain transduction, mouse strains, NeuN

INTRODUCTION

ADENO-ASSOCIATED VIRUS (AAV) has emerged as an important vector candidate for delivering targeting sequences for a broad range of neurodegenerative diseases, including Parkinson's disease, Huntington's disease, and Alzheimer's disease.¹⁻³ AAV has 13 serotypes, more than 100 naturally occurring variants, and an expanding library of modified capsids, which can be used as gene delivery vehicles. However, selecting an appropriate capsid from the array of AAV serotypes/variants can be difficult since different AAV capsids have a variety of tissue transduction abilities, which only partially result from the interaction with different receptors or coreceptors on the targeted cells.⁴⁻⁶

While AAV vectors have been effectively used to target several different cell types, including retinal pigmented epithelial cells and hepatocytes, extensive effort has also been put toward identifying specific AAV capsids with different phenotypes for targeting various cell types in the brain. However, conflicting results regarding cell targeting efficiency in the brain have been reported in studies using mouse models. This may be due to utilization of a variety of different rodent strains among the different studies.⁷⁻¹⁰ Furthermore, the remarkable brain transduction of an AAV9 variant named PHP.B following intravenous infusion was subsequently found to be limited to mice from a C57BL/6J background.¹¹ PHP.B does not show enhanced

*Correspondence: Dr. Chengwen Li, Gene Therapy Center, University of North Carolina at Chapel Hill, Chapel Hill, 104 Manning Drive, 7007 Thurston-Bowles, CB #7352, Chapel Hill, NC 27599. E-mail: chengwen_li@med.unc.edu

transduction in BALB/cJ mice or nonhuman primates, which has been linked to different Ly6a haplotypes, at least between mouse species.¹² In addition, genetic variations among multiple strains established by the Collaborative Cross were identified to contribute to the differential transduction by lentiviral vector-delivered luciferase.¹³ Given the current literature, it is apparent that a systematic characterization of the transduction properties of AAV serotypes in the central nervous system of multiple rodent strains remains critically unaddressed.

Recently, gene therapy has shown gains in overall success and promising results in clinical trials for a wide range of genetic diseases; however, significant variations have always existed in the efficacy and safety measured among treated patients within each clinical study.^{14–16} Furthermore, the various responses in individual patients, especially certain immunological effects, were not predicted by the preclinical studies.¹⁶ The use of single animal strains in preclinical studies may have led to an underestimation of the variability in efficacy and safety.

Here, we studied the impact of the host genetic background on AAV transduction properties with different AAV serotypes in different mouse strains. Two common laboratory mouse strains, C57BL/6J and FVB/N, were transduced with several popular AAV serotypes (AAV2, 5, 7, 8, and 9). We chose these serotypes due to their historical precedent (AAV2), their popular use in the brain (AAV9), and observations from our laboratory of robust brain transduction with serotypes 5, 7, and 8. The C57BL/6J mouse strain is the most widely used inbred strain in preclinical research. Furthermore, this strain contains a permissive background for maximal expression of most mutations and is commonly used in the production of transgenic mice. FVB inbred mice are also ideal for generating transgenic mouse models, such as the YAC128 strain, which was developed to study Huntington's disease, because these mice have prominent pronuclei that enable more efficient transgene microinjection and high reproductive performance¹⁷; hence, both mouse strains are relevant to current preclinical gene therapy studies. We found that different AAV capsids possess differential transduction properties and that the host genetic background strongly affects the ability of AAV vectors to transduce brain tissue after intrastriatal injection. Our data suggest that the strain-specific differences in AAV vector-mediated brain transduction may contribute to the variable results observed in individual clinical patients following

gene therapy. This study also highlights the importance of identifying specific genetic factors that could impact AAV brain transduction.

RESULTS

Comparison of brain enhanced green fluorescent protein (EGFP) expression in the striatum conferred by different AAV serotypes in two strains of mice

We analyzed transgene enhanced green fluorescent protein (EGFP) expression in the brain, 5 weeks after intrastriatal injection with AAV2, 5, 7, 8, and 9 in C57BL/6 and FVB mice. As shown in Fig. 1A, all serotypes are capable of transducing brain tissue efficiently in both strains of mice. However, for C57, three serotypes AAV5, AAV7, and AAV9 transduced a relatively larger area than serotypes AAV2 and AAV8, and also resulted in a higher fluorescence index (Fig. 1A–C). The fluorescence index indicates the total EGFP fluorescence, including both the number of pixels with positive GFP expression and the levels of GFP signal in each pixel. In C57 mice, AAV5 is the most widespread virus (Fig. 1C), but has less or similar total EGFP expression in transduced cells as AAV7 or AAV9 (Fig. 1B). In contrast, the FVB mice did not display a significant difference in total EGFP expression among the five AAV serotypes, although AAV5 transduced a significantly larger area (Fig. 1A–C). When comparing between the two species of mice, AAV7 produced significantly more EGFP in C57 mice compared with EGFP in FVB mice (analysis of variance [ANOVA]; $p < 0.05$, Fig. 1B). In general, FVB mice did not show significant differences between the serotypes with regard to fluorescent index, whereas C57s showed significant differences between serotypes, with AAV5, AAV7, and AAV9 being the highest (Fig. 1B). There were significant differences between the serotypes when looking at the spread of transduction, with AAVs 5, 7, and 9 being the highest in both mouse strains, although only significantly so in C57s (Fig. 1C).

Ipsilateral and contralateral cortex EGFP expression

As the striatum receives axonal innervation from both the ipsilateral and contralateral cortices through corticostriatal projections, retrograde axonal transport after striatal AAV injection could result in EGFP expression in cortical neurons in both injected and noninjected hemispheres. In our study, we found cortical neuron EGFP expression in most of the AAV-injected mice, although to varying degrees (Fig. 2A, B). In general, the cortex in C57 mice had stronger EGFP signal on both sides of the brain than in FVB mice (Fig. 2C). EGFP expression from

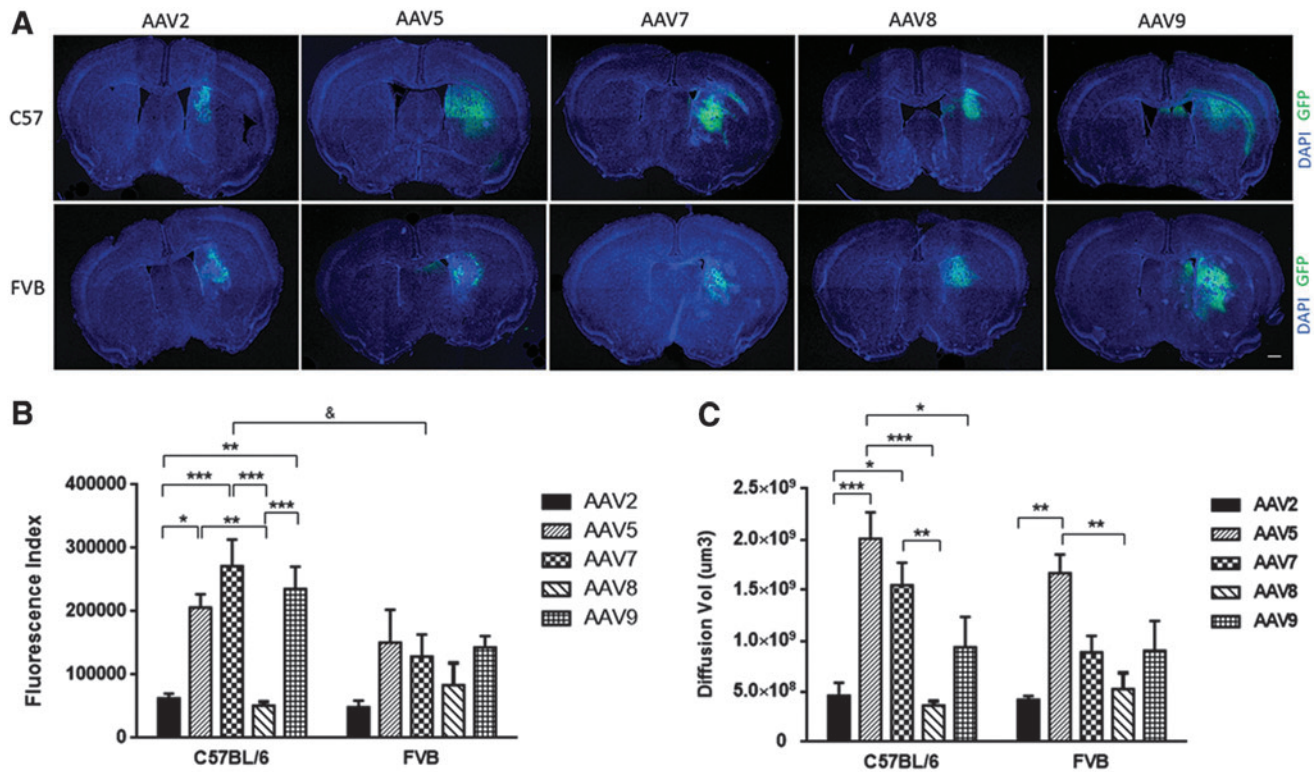


Figure 1. Transduction efficiency of AAV2, 5, 7, 8, and 9 in brains of C57BL/6 and FVB mice 5 weeks following AAV injection. **(A)** Representative confocal fluorescence images of caudate putamen (CPU) in C57BL/6 (*Top*) or FVB (*Bottom*) mice injected with various AAV serotypes (objective 2 \times ; scale bar is 500 μ m). *Green*: EGFP expression. *Blue*: DAPI staining. **(B)** Fluorescence index analysis of EGFP expression conferred by AAV stereotypes in C57 and FVB mice. **(C)** Quantity analysis of AAV serotype transduction by diffusion volume (μ m³) in C57 and FVB mice. All bars represent mean \pm SEM. $n=4-5$ in each group. * $p<0.05$, ** $p<0.01$, *** $p<0.001$ compared within C57 or FVB group. $\delta p<0.05$ compared between C57 and FVB with AAV7 injection. AAV, adeno-associated virus; DAPI, 4',6-diamidino-2-phenylindole; EGFP, enhanced green fluorescent protein; SEM, standard error of the mean.

AAV7 in the ipsilateral cortex is significantly higher in C57 mice than all other serotypes in both strains of mice examined ($p<0.05$, Fig. 2C). On the contralateral side, AAV5 resulted in significantly more cortical neurons expressing EGFP in C57 mice than in FVB mice ($p<0.001$, Fig. 2D). AAV5 also exceeds all other serotypes in cortical EGFP expression in both C57 and FVB mice on both sides of the cortex, but particularly on the contralateral side, which may indicate a pronounced ability of AAV5 to infect axon termini (Fig. 2D). The quantification of retrograde trafficking events is complicated by EGFP expression arising from anterograde trafficking (or diffusion) of EGFP protein from neurons on the ipsilateral side that have axonal projections into the contralateral side. Since we measured total EGFP signal and diffusion volume, and did not count individual cell bodies, we were unable to distinguish between these two possibilities.

Cellular tropism of AAV vectors in C57 and FVB mice

AAV capsids have different cellular tropisms driven, in part, by differences in receptor binding.

Since the brain comprised of a collection of different cell types, including various neurons and glial cells, we sought to identify cell-type differences in transduction between AAV serotypes and mouse strains. At 5 weeks postinjection, we removed, sectioned, and stained the brains of the mice injected with EGFP AAV vectors. By using the cell-type-specific markers NeuN (neuronal marker), GFAP (astrocyte marker), and olig-2 (oligodendrocyte marker), we were able to determine the cell-specific tropism of AAV serotypes 2, 5, 7, 8, and 9 in C57 and FVB mice. Three sections (each 40 μ m thick), which represented the central concentration of EGFP expression, were chosen per animal for quantification of colocalization with the cell-type-specific markers. We also found a lack of immunoreactivity of NeuN, which occurred using specific serotypes in both mouse strains. With the exception of those cells that had a loss of NeuN immunoreactivity, there is a higher percentage of transduction in neurons (40–60% of all EGFP transduced cells) when compared with transduction of astrocytes and oligodendrocytes (Fig. 3D–F). We excluded the animals that displayed a loss of NeuN immunore-

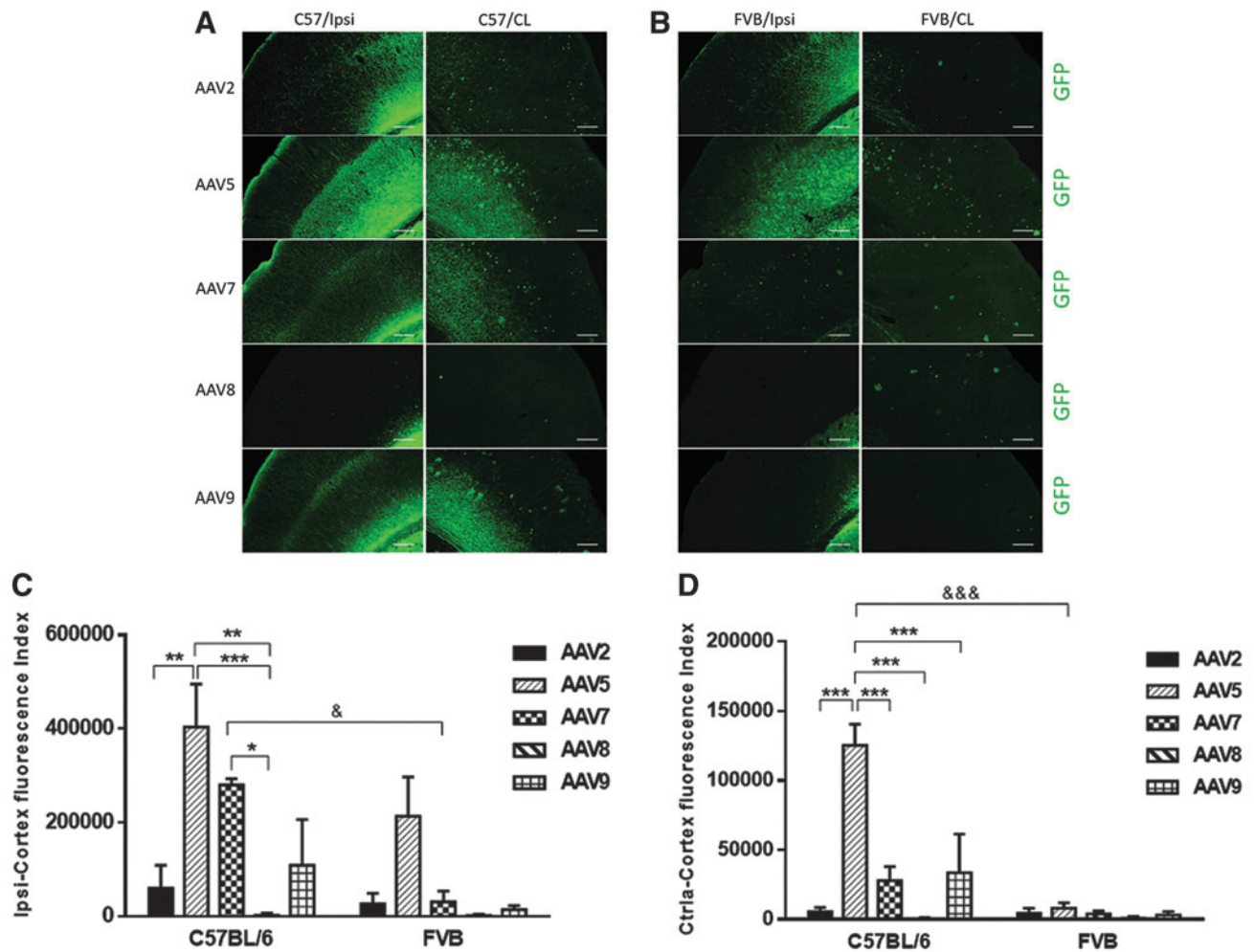


Figure 2. EGFP expression in ipsilateral (Ipsi) and contralateral (CL) cortex 5 weeks post-AAV vector injection in striatum. **(A, B)** Representative confocal images (objective 20 \times ; scale bar is 200 μ m) from both sides in C57 **(A)** and FVB **(B)** mice injected with various AAV serotypes. **(C, D)** Quantitative analysis of fluorescent index of the cortex EGFP expression from ipsilateral cortex **(C)** and contralateral cortex **(D)** in C57 and FVB mice. All bars represent mean \pm SEM. $n=3$ in each group. * $p<0.05$; ** $p<0.01$; *** $p<0.001$ compared within C57 or FVB group. & $p<0.05$; &&& $p<0.001$ compared between C57 and FVB with AAV7 injection.

activity in quantification of NeuN-positive cell colocalization, and found that AAV8 demonstrates less neuronal preference than AAV9 in C57 mice (* $p<0.05$, Fig. 3D). In FVB mice, a loss of NeuN immunoreactivity could be seen with the AAV serotypes tested except for AAV8, in which 60% of the EGFP-positive cells are neurons Fig. 3D). The transduction in astrocytes varied from $\sim 3\%$ to 4% with AAV9 to 14–19% with AAV5 in both strains (Fig. 3E). There is significantly more astrocyte transduction with AAV5 than with AAV7 and AAV9 in FVB mice (** $p<0.01$ or * $p<0.05$, Fig. 3E). Notably, each AAV serotype exhibited a similar amount of transduction in astrocytes in both C57 mice and FVB mice (Fig. 3E). AAV8 transduction resulted in $\sim 23\%$ of oligodendrocytes that were EGFP positive in C57 mice, which is significantly more ($p<0.001$; Fig. 3F) than that measured in

FVB mice (only 4.4%). In C57 mice, AAV7 also showed a high percentage of oligodendrocyte transduction, similar to AAV8. In contrast, in FVB mice, AAV7 transduced significantly more oligodendrocytes than AAV8 (* $p<0.05$; Fig. 3F). AAV8 displays the largest difference in oligodendrocyte transduction between the two strains of mice (Fig. 3F).

NeuN loss and rotarod behavioral testing results

In the course of determining neuronal cell tropism for the AAV serotypes, we found that the area of AAV transduction frequently also displayed a lack of NeuN staining that was not observed in uninjected or untransduced areas of the brain. This loss of NeuN immunostaining had both mouse strain- and serotype-specific differences, with the

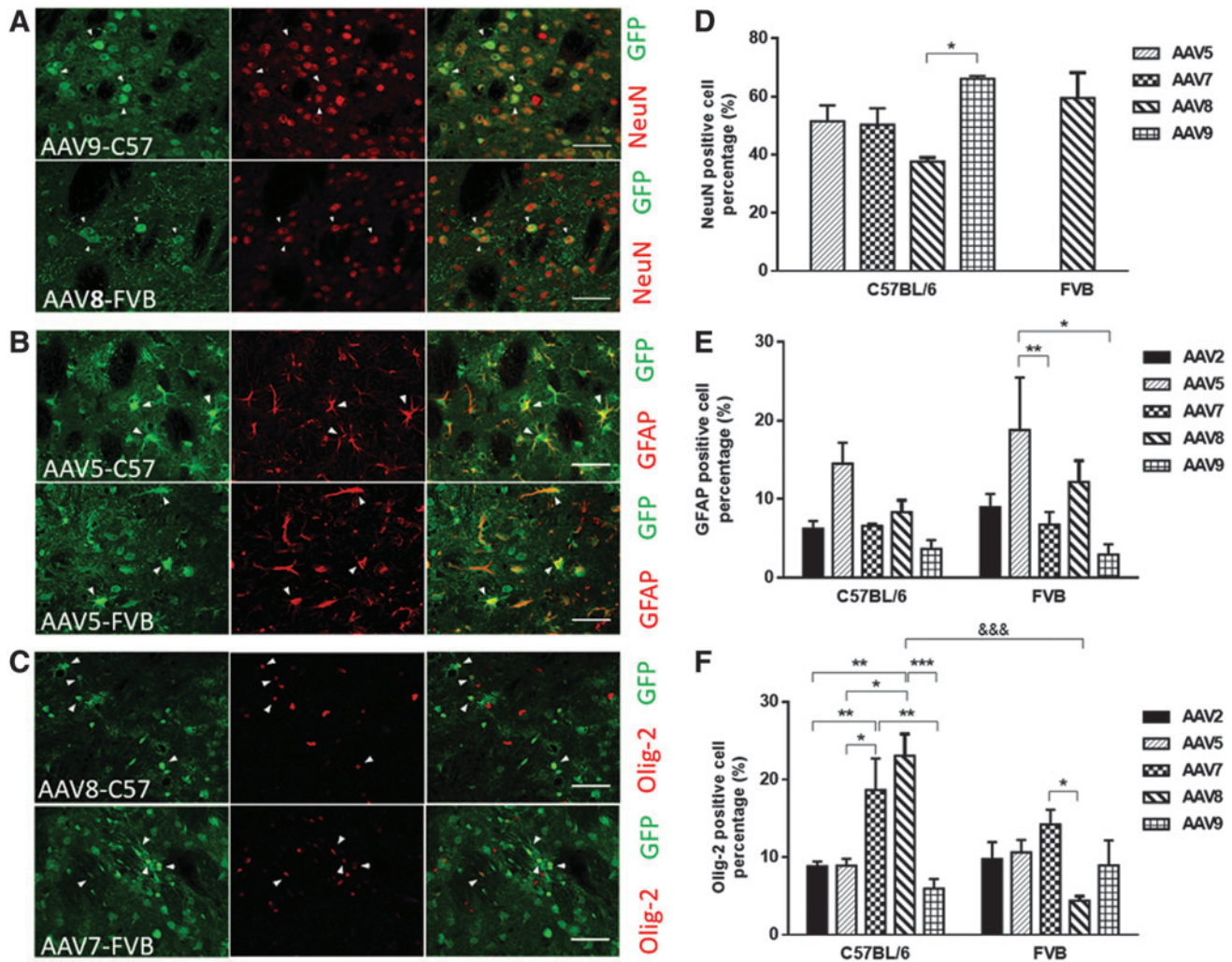


Figure 3. Cellular tropism of AAV2, 5, 7, 8, and 9 in C57 and FVB mice. The representative confocal images (objective 30 \times ; scale bar is 50 μ m) display the serotypes that have the most transduction in a specific cell type in either C57 or FVB mice. **(A)** EGFP colocalization with neuron marker NeuN; **(B)** EGFP colocalization with astrocyte marker GFAP; and **(C)** EGFP colocalization with oligodendrocyte marker Olig-2. The specific cell percentage is quantified by the percentage of the number of a specific marker-positive cell in total EGFP-positive cells. **(D-F)** Cell percentage quantifications for neurons, astrocytes, and oligodendrocytes. All bars represent mean \pm SEM. $n=3$ in each group. * $p<0.05$; ** $p<0.01$; *** $p<0.001$ compared within C57 or FVB group. &&& $p<0.001$ compared between C57 and FVB with AAV7 injection.

loss occurring more frequently in the FVB strain (Fig. 5A, B). Loss of NeuN is most prominent with AAV5 and AAV7 transduction in FVB mice, in which the whole striatum and adjacent cortex had extensive loss of NeuN immunoreactivity (Fig. 4A, C, F). Quantification of NeuN-positive cells in the ipsilateral half hemisphere, showed that AAV5- and AAV7-injected FVB mice had the least number of NeuN-positive cells (Fig. 5A), which also resulted in the smallest area with intact NeuN-positive signal (Fig. 5B). However, AAV5-EGFP did not induce any NeuN loss in C57 mice, although we did observe NeuN loss in one C57 mouse injected with AAV7-EGFP (Fig. 4B). Significant strain differences were found in NeuN immunoreactivity with the serotypes AAV5, AAV7, and AAV9. A portion

of AAV9-injected FVB mice also had a small area of NeuN loss (Fig. 4D), however, this loss was not observed in C57 mice. Most of the AAV2-injected mice in both strains had a small region of NeuN loss in the center of the viral EGFP expression site (Fig. 4A, B). Interestingly, NeuN immunoreactivity remained intact in AAV8-injected mice in both strains (Figs. 4E and 5A, B).

To evaluate if the loss of NeuN immunoreactivity could result in compromised animal behavior, we injected FVB mice with AAV7-GFP vectors as in the above serotype comparison study. These mice were then subjected to a rotarod test since motor deficits are the major symptoms if striatal neurons are lost or functionally damaged, as shown in Huntington's disease.¹⁸ However, we

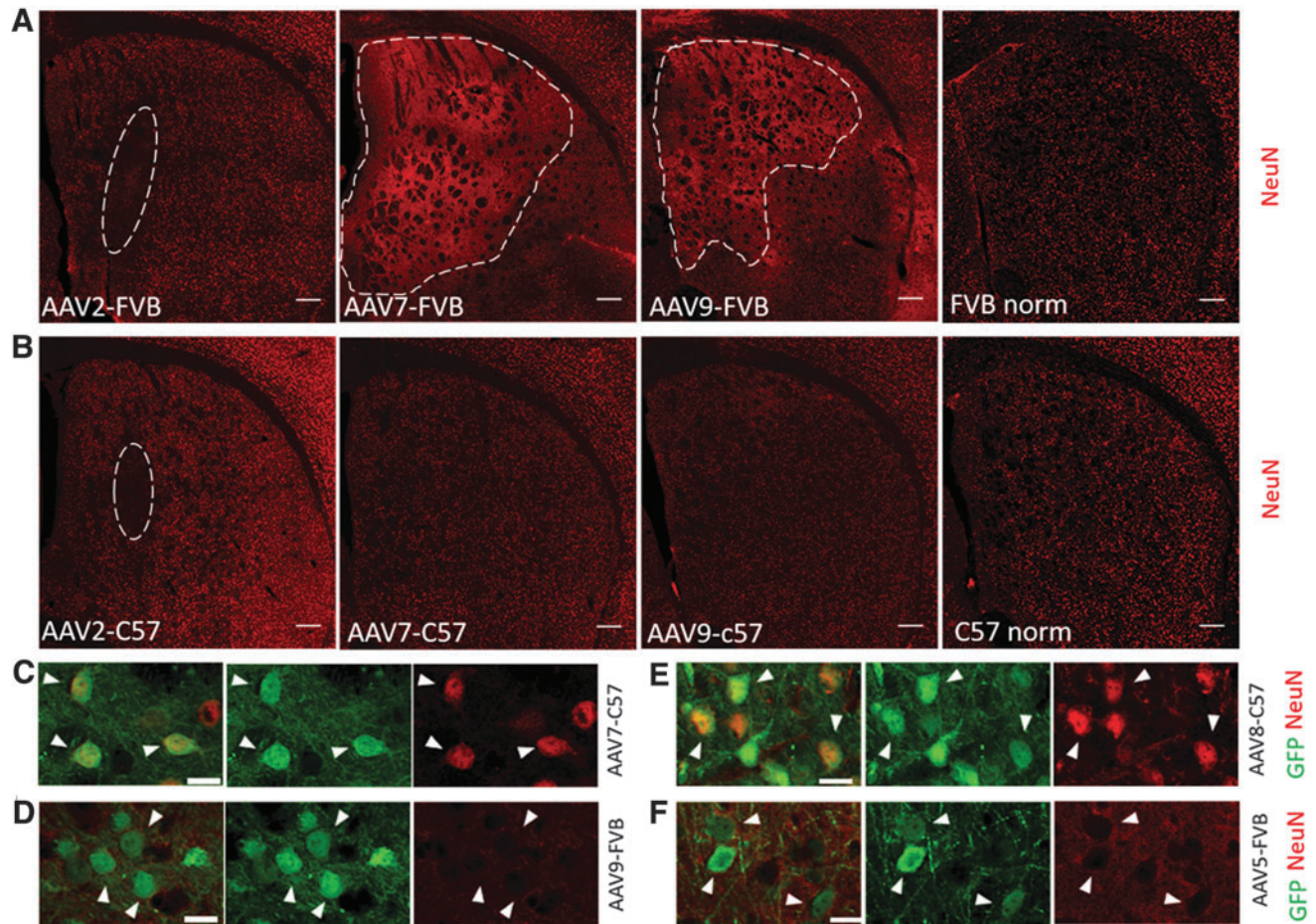


Figure 4. Loss of NeuN immunoreactivity in the ipsilateral striatum with injection of AAV-delivered EGFP. **(A, B)** Representative tiling confocal images showing either loss of NeuN immunofluorescence (the region of loss is *circled*), or NeuN immunofluorescence remained intact postinjection. Images of NeuN staining in normal untreated FVB or C57 mice also shown as control (20 \times ; scale bar is 200 μ m). **(C–F)** Higher magnification images (30 \times ; scale bar is 15 μ m) showing intact NeuN or loss of NeuN and corresponding EGFP expression for individual neurons in the striatum.

did not observe any significant reduction of motor performance in an accelerated rotarod test for AAV7-injected FVB mice, compared with normal untreated FVB mice (Fig. 5C). The AAV7-injected animals used for the behavioral study had a similar NeuN-positive cell density and similar NeuN loss area compared with AAV7-injected FVB mice in the serotype comparison study (Fig. 5D, E), which was significantly lower than untreated mice.

Medium spiny neuron transduction with AAVs-EGFP

The medium spiny neurons (MSNs) are the major type of neurons in the striatum and are frequently perturbed in Huntington's disease.¹⁸ Thus, we wanted to know if NeuN immunoreactivity loss could affect MSNs. As a marker for MSNs, we performed immunostaining for DARPP-32 and we found that in AAV5- or AAV7-injected FVB mice, which exhibited the most NeuN loss, DARPP-

32 immunoreactivity was also strongly reduced, and significantly fewer neurons were found to be positive for DARPP-32 staining overall (Fig. 6A; AAV7 data not shown). However, we could still observe normal neuron morphology from the EGFP signal, suggesting that while those neurons may lose NeuN and DARPP-32 immunoreactivity, they are still morphologically intact and able to express GFP. In contrast to that, in AAV9- or AAV2-injected FVB mice, we can find that some DARPP-32-positive neurons colocalize with EGFP expressing cells, but these neurons lack NeuN staining (Fig. 6B; AAV2 data not shown). In this situation, we speculate that the MSNs in the striatum were less affected by the injection of AAV2 or AAV9, since DARPP-32 immunoreactivity remained intact. AAV8-injected FVB mice, as well as the other animals without NeuN loss, show normal NeuN and DARPP-32 immunostaining patterns, which colocalize with EGFP expressing neurons (Fig. 6C).

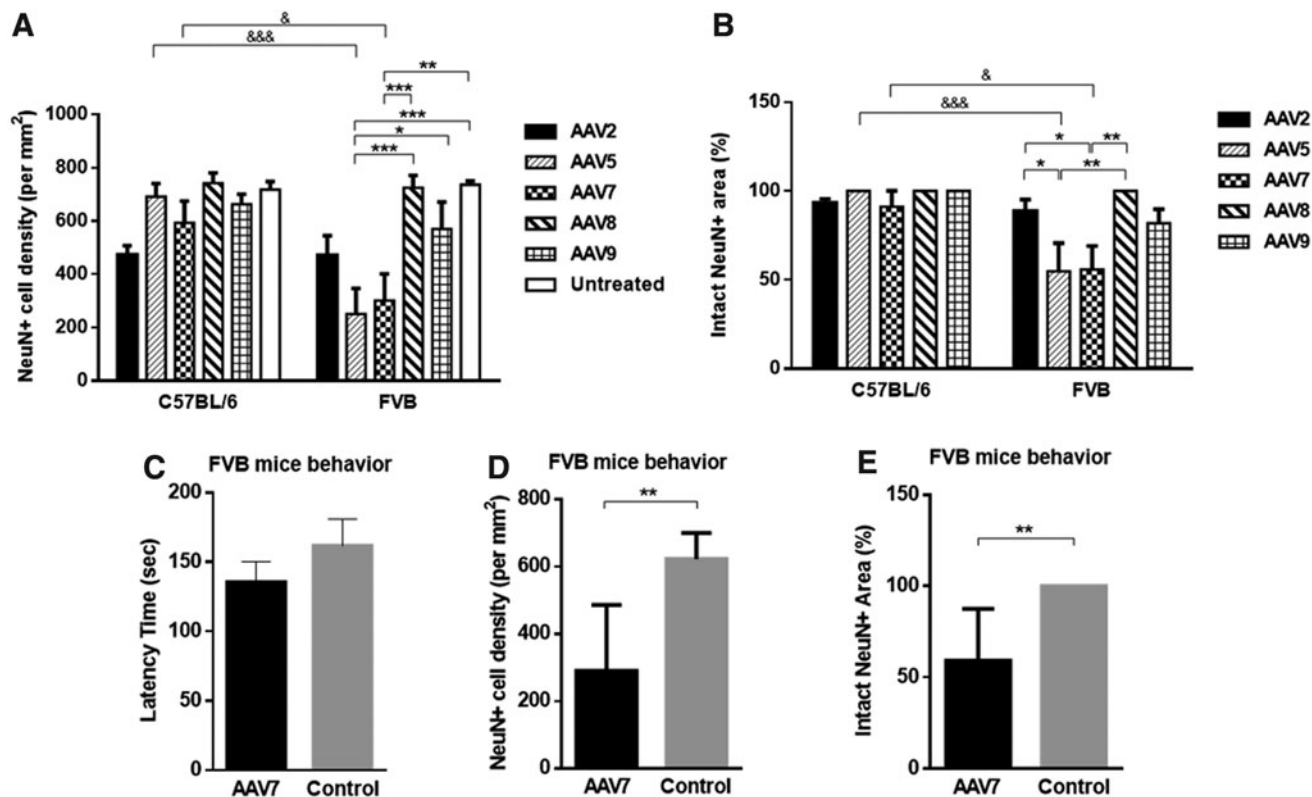


Figure 5. Quantitative analysis of NeuN immunoreactivity in ipsilateral striatum postinjection of varied AAV serotype-delivered EGFP. AAV7 and control FVB mice were subjected to behavioral study 5 weeks postinjection, and rotarod performance, as well as NeuN-positive cell density, and intact NeuN area were quantified to verify the consistency with a serotype comparison study. **(A)** Quantification of NeuN-positive cell density in ipsilateral half hemisphere. **(B)** Area percentage from intact NeuN immunofluorescence in ipsilateral half hemisphere. **(C)** Latency time in accelerating rotarod test in AAV7-EGFP-injected and nontreated control FVB mice. **(D, E)** NeuN-positive cell density **(D)** and intact NeuN area percentage **(E)** in ipsilateral half hemisphere in behavior study animal. All bars represent mean \pm SEM. $n=4-5$ in each group for **(A, B)**, $n=11$ (AAV7) and $n=6$ (control) for **(C)**, and $n=8$ (AAV7) and $n=6$ (control) for **(D, E)**. * $p < 0.05$; ** $p < 0.01$; *** $p < 0.001$ compared within C57 or FVB group. & $p < 0.05$; &&& $p < 0.001$ compared between C57 and FVB mice.

Activation of microglia

Microglia are the primary innate immune cells in the central nervous system (CNS) and microglia-mediated immune responses play an important role in the pathway leading to neuronal degeneration and death.^{19,20} Therefore, it was important to determine if microglia became activated in the AAV-EGFP-injected mice. To measure this activation level, we immunostained 40 μm sections of brain tissue with an antibody against Iba-1, which is a marker for microglia that becomes upregulated upon microglial activation (Fig. 7A–D). Quantification of the microglial fluorescence index in both ipsilateral and contralateral sides of the striatum was performed (Fig. 7E). The results showed that AAV5 and AAV7 induced a significant increase in the amount of Iba-1 expression, compared with the signal from the corresponding contralateral side of the same striatum (Fig. 7E). Representative confocal images showed a difference between AAV7-injected FVB and C57 mice (Fig. 7A–D). Note that although FVB mice did not have as much GFP ex-

pression in the injected striatum compared with the C57 mice, they do show significantly more levels of microglial activation (Fig. 7B, D). Due to a significantly low EGFP expression on the contralateral side of the striatum, we were able to use this region as an internal control to the ipsilateral side. In addition, we did not observe a significant difference in microglial signal in the contralateral side of the striatum in all of the mice.

DISCUSSION

We compared and analyzed the transduction properties of five widely used recombinant AAV (rAAV) vectors in two different strains of mice post intra-striatal injection. Extensive studies have been conducted for comparison of brain transduction efficiency and cellular tropism after intracerebral administration of AAV vectors and the results have been conflicting and complicated by utilization of varied animal strains. For instance, AAV8 was found to target only neurons in some

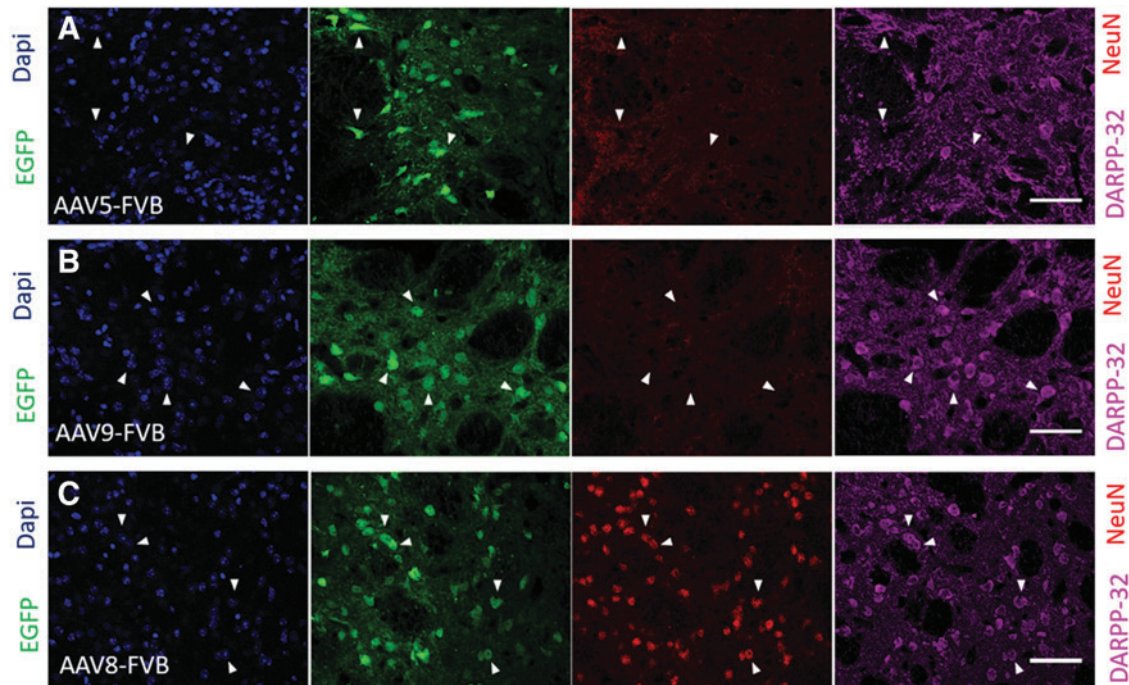


Figure 6. The varied levels of potential neuronal toxicity to medium spiny neurons in striatum after AAV-EGFP administration suggested by different NeuN and DARPP-32 immunoreactivity in FVB mice. **(A)** Loss of both NeuN and DARPP-32 immunofluorescence in AAV5-EGFP-injected FVB mice. **(B)** Loss of NeuN, but DARPP-32 signal remained intact, in AAV9-EGFP-injected FVB mice. **(C)** In AAV8-EGFP-injected FVB mice, both NeuN and DARPP-32 remained intact. Images were taken with 20 \times objective, scale bar is 50 μ m.

studies, but have preference for astrocytes over neurons in other studies.^{7–10} The conflicting data has also occurred with other serotypes including AAV2, 5 and 9.^{7,8,10} Therefore, it is important for variables to be constrained so that different AAV serotypes can be compared systematically. To our understanding, this is the first time that multiple rAAV vectors have been comprehensively compared simultaneously in two mouse strains. In our study, the five serotypes being tested can transduce a variety of different cell types in the brain. In general, AAV5 has more preference for targeting GFAP-positive astrocytes, which comprises 20% of all EGFP-positive cells, especially in the case of FVB mice. However, there is no significant difference in targeting of astrocytes between the two strains for each specific AAV serotype. Oligodendrocytes are the myelin-forming cells of the CNS.²¹ Our data showed that AAV8 and AAV7 transduced oligodendrocytes most efficiently in C57 mice with a transduction rate of 20% of total EGFP-positive cells. However, in FVB mice, AAV7 retained a high ability to transduce oligodendrocytes, but AAV8 had a diminished ability to target oligodendrocytes. For neuronal staining, the loss of NeuN immunoreactivity in several serotypes complicated the quantification of colocalization between NeuN- and EGFP-positive cells. In mice exhibiting normal

NeuN-staining, the majority of the EGFP signal was expressed in NeuN-positive neurons, although AAV8 had less neuron targeting specificity in C57 mice, which is consistent with the result that AAV8 targeted more oligodendrocytes in C57 mice. In regards to the comparison of transduction efficiency, a large discrepancy has also been reported across multiple studies.^{7,8,22,23} In this study, we found that in general, AAV5, 7 and 9 transduced the most brain tissue and have higher intracellular EGFP-expression than AAV2 and AAV8, for which the viral diffusion and EGFP-expression is more restricted. The widespread transduction of AAV5 is consistent with several other serotype comparison studies.^{7,10} Notably, when comparing the different serotypes, even though AAV5 has the largest area of transduction, it does not result in the strongest intracellular EGFP-expression. Instead, AAV9 and 7 have higher intracellular EGFP-expression in both mouse strains.

As the major neuronal cell type in the striatum, MSNs receive input from the cortex, thalamus, and brain stem, and the cortical fibers project to the dendritic spines to form asymmetric terminals.^{24,25} In this study, we observed that neuron soma on both sides of the cortex were labeled with EGFP. While the neurons in the ipsilateral side of the cortex were transduced by infection events near

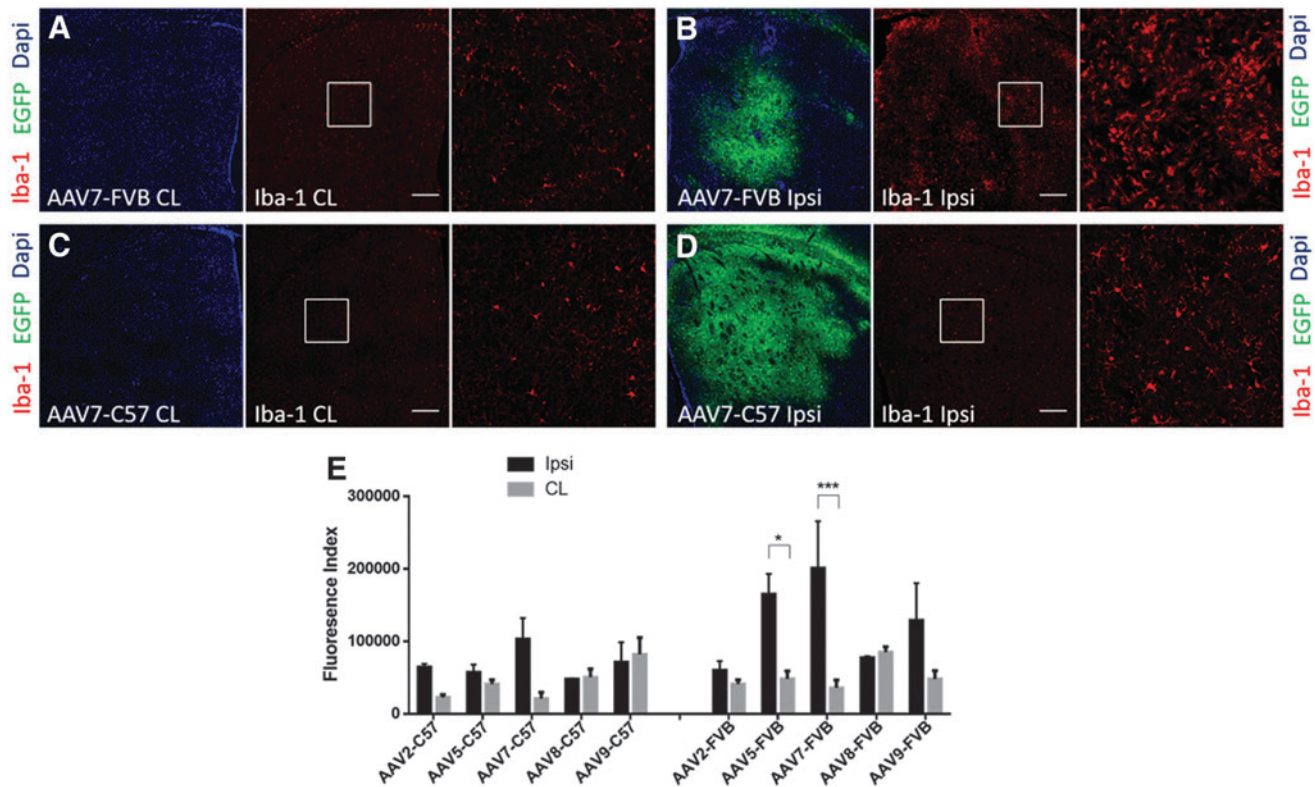


Figure 7. Differentiated microglial activation in ipsilateral and contralateral striatum with varied AAV-EGFP injection. Representative confocal images show the difference in Iba-1 immunostaining between FVB and C57 mice in contralateral (CL) and ipsilateral (Ipsi) sides. **(A)** Contralateral striatum and **(B)** ipsilateral striatum postinjection of AAV7-EGFP in FVB mice. **(C)** Contralateral striatum and **(D)** ipsilateral striatum postinjection of AAV7-EGFP in C57 mice. For each **(A–D)**, the *left image* is a layered image of both DAPI and EGFP. The *middle image* is Iba-1, and the *right image* is the zoom in image of boxed region in the *middle image*. The image was taken with objective 20 \times , scale bar is 250 μ m. **(E)** Quantification of fluorescence index of microglial level on both sides for all serotypes in C57 and FVB mice. All bars represent mean \pm SEM. $n=3$ in each group. * $p<0.05$; *** $p<0.001$ compared between contralateral and ipsilateral striatum in FVB mice with AAV5 and AAV7-EGFP injection.

the site of injection, the neurons with cell bodies residing on the contralateral side were likely transduced by striatal-cortical retrograde transport of AAV particles from infection events on the ipsilateral side. AAV5 was able to abundantly label neurons on both the ipsilateral and contralateral sides in both strains, suggesting a strong retrograde transport ability of AAV5, but again, this is complicated by neurons projecting from the ipsilateral side and maybe be only reflective of the ability of AAV5 to effectively transduce neurons, in general. Although, retrograde trafficking of AAV5 particles has been previously reported.⁷ From the current study, we see significantly less contralateral EGFP expression in FVB mice for AAV5, even though it has a similar amount of striatal transduction as in C57 mice. The interpretation of this might be associated with an increased vulnerability of neurons in FVB mice in response to transgene expression following AAV transduction.

NeuN is an exclusively neuronal marker, and anti-NeuN antibodies are able to identify most

types of neurons in the whole nervous system, with the exception of several cell types in the brain.²⁶ Several factors may lead to the lack of NeuN immunoreactivity, including neuronal injury post-hypoxia and brain injury.^{27–30} On the other hand, the abnormal synthesis of the NeuN protein or loss of NeuN protein antigenicity due to the lack of phosphorylation of the antibody binding sites can also result in a lack of NeuN immunoreactivity.^{31,32} Our study shows that FVB mice are more vulnerable to the loss of NeuN immunoreactivity associated with EGFP-delivered by AAV vectors, compared to C57 mice. There was extensive NeuN immunoreactivity loss in the striatum of AAV5 and AAV7-injected FVB mice. Additionally, AAV2 and AAV9 delivered EGFP induced partial NeuN loss in the striatum of FVB mice. We speculate that the striatal neurons in FVB mice may be more sensitive to the stress of foreign protein (EGFP) overexpression. However, AAV8 was an exception to this observation regarding NeuN loss since it robustly transduced neurons in FVB mice but did

not induce the NeuN loss seen with other serotypes. Similar to our results, Watakabe’s study has shown a loss of NeuN-positive cortical neurons of marmosets following the injection of CMV-driven AAV1 and AAV9-GFP.³³ Some studies have suggested a potential link of neuronal or glial toxicity with AAV-carrying transgene expression, such as GFP, both *in vivo* and *in vitro*.^{9,34,35} However, loss of NeuN immunoreactivity is not necessarily neuron loss and further study needs to be done to figure out the mechanisms behind the loss of NeuN immunoreactivity in this study. It is interesting that AAV2 transduced a similar amount of total brain tissue as AAV8, but still caused a small area of NeuN loss in both strains that was not observed with AAV8. Also, the strain-specific difference with NeuN immunoreactivity did not occur with AAV2 and AAV8. This might be associated with the interaction between AAV capsid and host tissue genetic environment.

DARPP-32 is a dopamine- and cAMP-regulated phosphoprotein, and is a major marker for MSNs in the striatum.³⁶ Our results indicated that in most of the AAV5- and AAV7- (data not shown) injected FVB mice, the region of NeuN loss also had a partial loss of DARPP-32 immunoreactivity, although EGFP-positive neurons still can be visualized with intact cell morphologies. In contrast to that, in AAV9- and AAV2- (data not shown) injected mice, the DARPP-32 immunoreactivity was intact in the region of NeuN loss, and some of the DARPP-32-positive signal actually colocalized with EGFP-positive cells. This demonstrates that AAV9 and AAV2 might only induce a partial or mild DARPP-32 dysfunction as compared to AAV5 and AAV7. A severe compromise of the function of striatal MSNs can cause motor coordination deficits.^{37,38} However, there is no significant decline in motor performance as shown in our accelerating rotarod testing³⁹ with AAV7-CBh-EGFP injection, even though this group of animals also demonstrated a similar level of NeuN immunoreactivity loss as AAV7 injected mice in the serotype comparison study. The behavior data suggested that the loss of NeuN as well as partial loss of DARPP-32 immunoreactivity in FVB mice has not compromised the major function of MSNs in the striatum following AAV5 and AAV7 injection.

Microglia are the primary resident immune cells in the CNS and are usually the first to be activated in response to tissue damage or brain infection.⁴⁰ The beneficial or detrimental role of microglial activation in neurological disorders remains to be elucidated; however, microglial activation is the major contributor to neuroinflammation in the

CNS.⁴¹ It is already known that neuroinflammation causes neurodegeneration in neurodegenerative diseases, including striatal dopaminergic degeneration in Parkinson’s disease.⁴² Our study has suggested a significant upregulation of microglial activation in the ipsilateral striatum of FVB mice following AAV5 and AAV7 injection, which is consistent with the significant lack of NeuN as well as DARPP-32 immunoreactivity observed in those mice. Therefore, it is reasonable for us to speculate that the loss of NeuN and DARPP-32 immunoreactivity may result from neuroinflammation caused by microglial activation. Whether other cells, such as T helper cells, have infiltrated into the brain and are involved in playing roles in the process of AAV-mediated NeuN and DARPP-32 loss still requires further study.

Again, the genetic background plays an important role in regulating the microglial activation and therefore in differentiating the transduction properties for AAV vectors in the brain. In Alzheimer’s research, APP processing and beta-amyloid levels were regulated according to various genetic backgrounds⁴³ and our results confirmed that C57Bl/6J mice have reduced microglial activity compared with mice with the FVB/N genetic background after injection with AAV vectors.⁴⁴

In this study, we compared five commonly used AAV serotypes with regard to each serotype’s brain transduction properties within the same strain, but most importantly, we differentiate the transduction of specific AAV serotypes between two different genomic backgrounds. The results of this study are summarized in Table 1, excluding the cell-specific transduction profiles, highlighting the differences we observed between the two strains of mice. These results suggest that we should use

Table 1. Summary of serotype differences between the two strains of mice

		AAV2	AAV5	AAV7	AAV8	AAV9
Total EGFP	C57	+	+++	+++	+	+++
	FVB	+	++	++	++	++
Spread volume	C57	+	+++	+++	+	++
	FVB	+	+++	++	+	++
Contralateral transduction	C57	+	+++	++	+	++
	FVB	+	++	+	+	+
Loss of NeuN	C57	+	-	-/+	-	-
	FVB	+	+++	+++	-	++
Microglial Ipsi/CL	C57	+	-	+	-	-
	FVB	+/-	+++	+++	-	++

Total EGFP, spread volume, contralateral transduction, loss of NeuN immunoreactivity, and microglial activation, indicated by relative Iba-1 ipsilateral to contralateral for each serotype in C57 and FVB mice, are summarized by using simple indicators from the lowest value in a group (+) to highest value in a group (+++).

AAV, adeno-associated virus; EGFP, enhanced green fluorescent protein; Ipsi/CL, ipsilateral/contralateral.

caution when evaluating an AAV vector's efficacy and safety with only one strain of mice and be aware that confounding data could occur if different genetic backgrounds of a disease model have been used by different studies. Therefore, it is our suggestion that preclinical evaluation of AAV-based vectors should involve the disease models in multiple genetic backgrounds when possible.

MATERIALS AND METHODS

Plasmid construction and rAAV production

The plasmid construction and rAAV production are performed by the UNC vector core. For packaging of rAAV vectors, the classical three-plasmid-based production method was used.²¹ Briefly, 293 cells were cotransfected with three plasmids consisting of an AAV helper plasmid (AAV2 Rep and the AAV Cap from serotypes AAV2, 5, 7, 8, or 9), a vector plasmid containing the ITRs from AAV2 flanking an EGFP transgene driven by the CBh promoter, and an adenoviral helper plasmid. Cells were harvested 72 h post-transfection and collected by centrifugation. Purification was performed using iodixanol gradient ultracentrifugation and further purified by column chromatography. Final preparations were dialyzed against phosphate-buffered saline (PBS) and adjusted to 1×10^{12} vg (viral genome) per milliliter for all the AAV vectors.

Animals and intracerebral viral injection

Six-week-old female C57 BL/6J and FVB/N mice were purchased from the Jackson Laboratory. For intracerebral viral injection, continual anesthesia was induced by isoflurane (1–2%) inhalation. The head of the mouse was fixed to the stereotaxic apparatus (KOPF Instruments, Tujunga, CA) and a small hole was made. The coordinates used for intrastriatal injection are anterior/posterior +0.9 mm, medial/lateral –1.5 mm, and dorsal/ventral –3.2 mm relative to bregma. One microliter of the viral vector was delivered by Hamilton syringe (5 μ L capacity) driven by a legato 130 syringe pump at a constant flow rate of 100 nL/min. Each animal received a total of 1×10^9 vg in a 1 μ L volume. The needle (33 gauge) was left in place for a further 7 min before being removed and the incision was sutured back together.

Immunostaining

All the viral-injected mice, except the mice used in the behavior study, were sacrificed 5 weeks after virus injection. The animals were transcardially perfused using PBS and 4% paraformaldehyde (PFA). Brains were dissected and immersed in 4%

PFA overnight. Fixed brains were transferred to 30% sucrose for cryoprotection. The brains were then cut on a cryostat (Leica CM 3050S) to 40- μ m-thick coronal slices. The slices were kept in a cryoprotectant reagent and stored at -20° . For immunofluorescent staining, the free floating brain slices were washed with PBS and then twice with tris-buffered saline (TBS) containing 0.05% Triton X-100 (washing buffer). Then the slices were permeabilized with TBS containing 0.5% Triton-X 100 for 20 min. After that, the slices were incubated in blocking buffer (TBS, 3% donkey serum, and 0.5% Triton X-100) for 1 h at room temperature, and followed by incubation with primary antibodies in blocking buffer at 4°C overnight. Primary antibodies were used as follows: NeuN (mouse; Millipore/Sigma #MAB377; dilution 1:100); GFAP (rat; Thermo Fisher #13-0300; dilution 1:500); Iba-1 (rabbit; Wako; #019-19741; dilution 1:500); Olig-2 (rabbit; Millipore/Sigma, #AB9610; dilution 1:400); and DARPP-32 (rabbit; Cell Signal, #2306; dilution 1:400). On the following day, the brain sections were rinsed three times in washing buffer and followed by incubation with secondary antibodies conjugated with the appropriate fluorescent dyes (Alexa Fluor 488, Alexa Fluor 594, or 647; Jackson ImmunoResearch) for 2 h at room temperature. Finally, the sections were rinsed 3 times in washing buffer, followed by DAPI, 4',6-diamidino-2-phenylindole (DAPI) staining for 15 min, and mounted onto positively charged glass slides using antifading mounting media (Thermo Fisher, Pro-Long gold antifade).

Confocal imaging and data analysis

Coronal sections through the entire striatum were collected in a serial order. Images were acquired by an Olympus FluoView 3000RS confocal microscope (Olympus Corporation, Tokyo, Japan) with $2 \times / 0.08$ (magnification/N.A.), $20 \times / 0.75$, or $30 \times / 1.05$ (silicone oil) objectives in the UNC Neuroscience Center Microscopy Core facility. Tiled images with z-stacks (1.5- μ m intervals) were acquired and stitched using Olympus FluoView software. ImageJ (<http://rsbweb.nih.gov/ij/>) or Imaris (Bitplane) software was used for quantification. For fluorescence index calculations, the five serial slices (240- μ m-thick sections) with the highest viral EGFP expression were identified and the EGFP expression level was quantified. The fluorescence index was calculated as the sum EGFP signal intensity of all of the pixels determined to have a positive signal (thresholded above background level expression determined from the average of three nonexpressing regions within the

same image). The single slice with the highest viral EGFP expression was chosen to be a representative of each animal. Diffusion volumes were quantified using the volume of positive EGFP signals (determined to be above the background level threshold) from five serial slices with the highest EGFP expression levels. Colocalization was quantified with Imaris software using Spot segmentation on the DAPI signal, in an imaging size of $826.156 \times 829.47 \times 10.5 \mu\text{m}$. The percentage of cells positive for a specific marker was calculated as the total number of specific marker-positive neurons that colocalized with EGFP expressing neurons divided by the total number of EGFP expressing neurons. The NeuN-positive cell numbers were quantified in the ipsilateral half hemisphere of the brain, and the microglial fluorescence index was calculated in the striatum region.

Accelerating rotarod test

AAV7-injected FVB mice and untreated FVB mice were subjected to behavior testing of accelerating rotarod in the UNC behavior core facility. Mice were placed on a cylinder that slowly accelerated to a constant rotating speed. For each trial, revolutions per minute (rpm) are set at an initial value of 3, with a progressive increase to a maximum of 30 rpm across 5 min, the maximum trial length. The mice were first trained using three trials, with 45 s between each trial. Then, the mice were evaluated with two trials for their motor performance. Measures are taken of the latency for the mouse to fall from the top of the rotating barrel.

Statistics

All statistical analyses were performed using GraphPad software. For the behavioral testing animal, NeuN cell density, intact NeuN area percentage, and rotarod test were performed using unpaired two-tailed Student's *t*-tests. For all the other statistics, two-way ANOVA followed by multiple comparisons was used.

REFERENCES

1. Axelsen TM, Woldbye DPD. Gene therapy for Parkinson's disease, An Update. *J Parkinsons Dis* 2018;8:195–215.
2. Hocquemiller M, Giersch L, Audrain M, et al. Adeno-associated virus-based gene therapy for CNS diseases. *Hum Gene Ther* 2016;27:478–496.
3. Wild EJ, Tabrizi SJ. Therapies targeting DNA and RNA in Huntington's disease. *Lancet Neurol* 2017; 16:837–847.
4. Grimm D, Buning H. Small but increasingly mighty: latest advances in AAV vector research, design, and evolution. *Hum Gene Ther* 2017;28:1075–1086.
5. Pillay S, Meyer NL, Puschnik AS, et al. An essential receptor for adeno-associated virus infection. *Nature* 2016;530:108–112.
6. Summerford C, Bartlett JS, Samulski RJ. AlphaVbeta5 integrin: a co-receptor for adeno-associated virus type 2 infection. *Nat Med* 1999; 5:78–82.
7. Aschauer DF, Kreuz S, Rumpel S. Analysis of transduction efficiency, tropism and axonal transport of AAV serotypes 1, 2, 5, 6, 8 and 9 in the mouse brain. *PLoS One* 2013;8:e76310.
8. Cearley CN, Wolfe JH. Transduction characteristics of adeno-associated virus vectors expressing cap serotypes 7, 8, 9, and Rh10 in the mouse brain. *Mol Ther* 2006;13:528–537.

ACKNOWLEDGMENTS

The authors thank the Mouse Behavioral Phenotyping Core for help in designing and conducting the mouse behavior study, and the funding for the core, which is supported by the Eunice Kennedy Shriver National Institute of Child Health and Human Development (U54 HD079124). They acknowledge that the microscopy was performed at the Neuroscience Center Microscopy Core Facility, supported, in part, by funding from the NIH-NINDS Neuroscience Center Support Grant P30 NS045892 and the NIH-NICHD Intellectual and Developmental Disabilities Research Center Support Grant U54 HD079124.

AUTHORS' CONTRIBUTIONS

Conceptualization, C.L. and T.H.; Methodology, T.H. and M.S.I.; Investigation, T.H., L.F.E., C.L., and N.E.H.; Writing—Original draft, T.H.; Writing—Review and Editing, M.S.I., L.F.E., C.L., and R.J.S.; Funding acquisition, C.L.; Resources, C.L., R.J.S.; and Supervision, C.L.

AUTHOR DISCLOSURE

R.J.S. is the founder and a shareholder of Asklepios BioPharmaceutical. He receives research support through the University of North Carolina from Asklepios BioPharmaceutical. He holds patents that have been licensed by UNC to Asklepios BioPharmaceutical, for which he receives royalties. He has consulted for Baxter Health care and has received payment for speaking.

FUNDING INFORMATION

This work was supported by the National Institutes of Health Grants R01AI117408 and R01HL125749 (to C.L.), and P01HL112761 and R01AI072176 (to R.J.S.).

9. Klein RL, Dayton RD, Leidenheimer NJ, et al. Efficient neuronal gene transfer with AAV8 leads to neurotoxic levels of tau or green fluorescent proteins. *Mol Ther* 2006;13:517–527.
10. Taymans JM, Vandenberghe LH, Haute CV, et al. Comparative analysis of adeno-associated viral vector serotypes 1, 2, 5, 7, and 8 in mouse brain. *Hum Gene Ther* 2007;18:195–206.
11. Hordeaux J, Wang Q, Katz N, et al. The neurotropic properties of AAV-PHP.B are limited to C57BL/6J mice. *Mol Ther* 2018;26:664–668.
12. Hordeaux J, Yuan Y, Clark PM, et al. The GPI-linked protein LY6A drives AAV-PHP.B transport across the blood-brain barrier. *Mol Ther* 2019;27:912–921.
13. Suwanmanee T, Ferris MT, Hu P, et al. Toward personalized gene therapy: characterizing the host genetic control of lentiviral-vector-mediated hepatic gene delivery. *Mol Ther Methods Clin Dev* 2017;5:83–92.
14. Hacein-Bey-Abina S, von Kalle C, Schmidt M, et al. A serious adverse event after successful gene therapy for X-linked severe combined immunodeficiency. *N Engl J Med* 2003;348:255–256.
15. Manno CS, Pierce GF, Arruda VR, et al. Successful transduction of liver in hemophilia by AAV-Factor IX and limitations imposed by the host immune response. *Nat Med* 2006;12:342–347.
16. Morgan RA, Yang JC, Kitano M, et al. Case report of a serious adverse event following the administration of T cells transduced with a chimeric antigen receptor recognizing ERBB2. *Mol Ther* 2010;18:843–851.
17. Taketo M, Schroeder AC, Mobraaten LE, et al. FVB/N: an inbred mouse strain preferable for transgenic analyses. *Proc Natl Acad Sci U S A* 1991;88:2065–2069.
18. Bates GP, Dorsey R, Gusella JF, et al. Huntington disease. *Nat Rev Dis Primers* 2015;1:15005.
19. Hansen DV, Hanson JE, Sheng M. Microglia in Alzheimer's disease. *J Cell Biol* 2018;217:459–472.
20. Brown GC, Neher JJ. Microglial phagocytosis of live neurons. *Nat Rev Neurosci* 2014;15:209–216.
21. Bradl M, Lassmann H. Oligodendrocytes: biology and pathology. *Acta Neuropathol* 2010;119:37–53.
22. Broekman ML, Comer LA, Hyman BT, et al. Adeno-associated virus vectors serotyped with AAV8 capsid are more efficient than AAV-1 or -2 serotypes for widespread gene delivery to the neonatal mouse brain. *Neuroscience* 2006;138:501–510.
23. Dodge JC, Clarke J, Song A, et al. Gene transfer of human acid sphingomyelinase corrects neuropathology and motor deficits in a mouse model of Niemann-Pick type A disease. *Proc Natl Acad Sci U S A* 2005;102:17822–17827.
24. Haber SN. Corticostriatal circuitry. *Dialogues Clin Neurosci* 2016;18:7–21.
25. Somogyi P, Bolam JP, Smith AD. Monosynaptic cortical input and local axon collaterals of identified striatonigral neurons. A light and electron microscopic study using the Golgi-peroxidase transport-degeneration procedure. *J Comp Neurol* 1981;195:567–584.
26. Guse'nikova VV, Korzhevskiy DE. NeuN as a neuronal nuclear antigen and neuron differentiation marker. *Acta Naturae* 2015;7:42–47.
27. Davoli MA, Fourtounis J, Tam J, et al. Immunohistochemical and biochemical assessment of caspase-3 activation and DNA fragmentation following transient focal ischemia in the rat. *Neuroscience* 2002;115:125–136.
28. Igarashi T, Huang TT, Noble LJ. Regional vulnerability after traumatic brain injury: gender differences in mice that overexpress human copper, zinc superoxide dismutase. *Exp Neurol* 2001;172:332–341.
29. McPhail LT, McBride CB, McGraw J, et al. Axotomy abolishes NeuN expression in facial but not rubrospinal neurons. *Exp Neurol* 2004;185:182–190.
30. Unal-Cevik I, Kiling M, Gursoy-Ozdemir Y, et al. Loss of NeuN immunoreactivity after cerebral ischemia does not indicate neuronal cell loss: a cautionary note. *Brain Res* 2004;1015:169–174.
31. Lind D, Franken S, Kappler J, et al. Characterization of the neuronal marker NeuN as a multiply phosphorylated antigen with discrete subcellular localization. *J Neurosci Res* 2005;79:295–302.
32. Maxeiner S, Glassmann A, Kao HT, et al. The molecular basis of the specificity and cross-reactivity of the NeuN epitope of the neuron-specific splicing regulator, Rbfox3. *Histochem Cell Biol* 2014;141:43–55.
33. Watakabe A, Ohtsuka M, Kinoshita M, et al. Comparative analyses of adeno-associated viral vector serotypes 1, 2, 5, 8 and 9 in marmoset, mouse and macaque cerebral cortex. *Neurosci Res* 2015;93:144–157.
34. Albert K, Voutilainen MH, Domanskyi A, et al. AAV vector-mediated gene delivery to substantia nigra dopamine neurons: implications for gene therapy and disease models. *Genes (Basel)* 2017;8:E63.
35. Howard DB, Powers K, Wang Y, et al. Tropism and toxicity of adeno-associated viral vector serotypes 1, 2, 5, 6, 7, 8, and 9 in rat neurons and glia in vitro. *Virology* 2008;372:24–34.
36. Svenningsson P, Nishi A, Fisone G, et al. DARPP-32: an integrator of neurotransmission. *Annu Rev Pharmacol Toxicol* 2004;44:269–296.
37. Dang MT, Yokoi F, Yin HH, et al. Disrupted motor learning and long-term synaptic plasticity in mice lacking NMDAR1 in the striatum. *Proc Natl Acad Sci U S A* 2006;103:15254–15259.
38. Reinius B, Blunder M, Brett FM, et al. Conditional targeting of medium spiny neurons in the striatal matrix. *Front Behav Neurosci* 2015;9:71.
39. Dunham NW, Miya TS. A note on a simple apparatus for detecting neurological deficit in rats and mice. *J Am Pharm Assoc Am Pharm Assoc* 1957;46:208–209.
40. Stertz L, Magalhaes PV, Kapczinski F. Is bipolar disorder an inflammatory condition? The relevance of microglial activation. *Curr Opin Psychiatry* 2013;26:19–26.
41. Streit WJ, Mrak RE, Griffin WS. Microglia and neuroinflammation: a pathological perspective. *J Neuroinflammation* 2004;1:14.
42. Kaur K, Gill JS, Bansal PK, et al. Neuroinflammation—a major cause for striatal dopaminergic degeneration in Parkinson's disease. *J Neurol Sci* 2017;381:308–314.
43. Lehman EJ, Kulnane LS, Gao Y, et al. Genetic background regulates beta-amyloid precursor protein processing and beta-amyloid deposition in the mouse. *Hum Mol Genet* 2003;12:2949–2956.
44. Frohlich C, Paarmann K, Steffen J, et al. Genomic background-related activation of microglia and reduced beta-amyloidosis in a mouse model of Alzheimer's disease. *Eur J Microbiol Immunol (Bp)* 2013;3:21–27.

Received for publication February 7, 2019;
accepted after revision July 18, 2019.

Published online: November 20, 2019.